Encyclopedia of Earthquake Engineering
DOI 10.1007/978-3-642-36197-5_100-1

Probability Seismic Hazard Mapping of Taiwan

Chin-Tung Cheng[a], Pao-Shan Hsieh[a], Po-Shen Lin[a], Yin-Tung Yen[a] and Chung-Han Chan[b,c]*
[a]Disaster Prevention Technology Research Center, Sinotech Engineering Consultants, Inc., Taipei, Taiwan, ROC
[b]Department of Geosciences, National Taiwan University, Taipei, Taiwan, ROC
[c]Earth Observatory of Singapore, Nanyang Technological University, Singapore, Singapore

Synonyms

Hazard curve; Hazard map; Probabilistic seismic hazard assessment; Seismic hazard mitigation; Taiwan

Introduction

Studies on seismic hazard mitigation are important for seismologists, earthquake engineers, and related scientists. Among studies, probabilistic seismic hazard assessments (PSHAs) provide the probability of exceedance for a specific ground motion level during a time interval (see entry "► Probabilistic Seismic Hazard Assessment: An Overview"). PSHA results can provide a key reference for the determination of hazard mitigation policies related to building codes and the site selection of pubic structures. Therefore, multidisciplinary scientists have attempted to build reliable systems for PSHAs.

Due to the plate boundary between the Eurasian and Philippine Sea Plates, Taiwan has a high earthquake activity (Fig. 1) (see entry "► Earthquakes and Tectonics: An Observation from Taiwan"). In this region, devastating earthquakes lead to a loss of property and human life. Therefore, it is essential to develop a means of seismic hazard mitigation. One practical approach is to build a seismic hazard assessment system. Over the past few years, several studies have evaluated seismic hazards for Taiwan. For example, the Global Seismic Hazard Assessment Program (GSHAP, http://www.seismo.ethz.ch/static/GSHAP/) obtained a global probabilistic seismic hazard map that included Taiwan. However, this work employed earthquake catalogs obtained from global seismic networks rather than a detailed seismicity catalog from Taiwan. Another application was proposed by Campbell et al. (2002) who utilized seismic catalogs, active fault parameters, and ground motion prediction equations (GMPEs) for the world, the United States, and Taiwan. Cheng et al. (2007) evaluated seismic hazards for Taiwan and proposed a hazard map by integrating a catalog from a local network, active fault parameters, and seismogenic zones in Taiwan. Such studies are crucial for understanding seismic hazards in Taiwan. However, following these studies, many parameters and the database for seismic hazard assessments, such as understanding the tectonic setting, the distribution of active faults, GMPEs, and earthquake catalogs, have been revised and/or updated. By employing state-of-the-art parameters, an evaluation of seismic hazards can be more precise.

Seismic hazards for Taiwan are reevaluated through the PSHA approach as proposed by Cornell (1968). According to this approach, parameters for seismogenic sources, which may result in seismic hazards, are required. Several seismogenic sources were characterized, including shallow regional sources, deep regional sources, crustal active fault sources, subduction intraslab sources, and subduction interface sources. The parameters for each source are discussed according to information from the tectonic setting, geology, geomorphology, geophysics, and earthquake catalog and present the results in the form

*Email: cchan@ntu.edu.tw
*Email: chchan@ntu.edu.sg

DOI 10.1007/978-3-642-36197-5_100-1

of hazard maps and hazard curves. The results are compared with those proposed by previous studies and discuss their applicability for the future.

Methodologies and Seismic Activity Models

The PSHA Approach

The applied approach of PSHA was first developed by Cornell (1968) (see entry "Earthquakes and Tectonics: Probabilistic Seismic Hazard Assessment: An Overview"). According to the description of Kramer (1996), seismic hazards based on this approach can be assessed, as follows:

$$P[Y > y^*] = \iint P[Y > y^*|m, r] f_M(m) f_R(r) dmdr, \tag{1}$$

where $P[Y > y^*]$ is the probability, P, for a given ground motion parameter, Y, which exceeds a specific value, y^* $P[Y > y^*|m, r]$ is the probability conditional on an earthquake with magnitude, m, imparted by a seismogenic source with the closest distance, r, between the site of interest and seismogenic source; and $f_M(m)$ and $f_R(r)$ are the probability density functions for magnitude and distance, respectively.

If there are N_S potential seismogenic sources near the site of interest, each of which has an average rate, v_i. The total average exceedance rate, λ_{y^0}, for the region can be presented as follows:

$$\lambda_{y^0} = \sum_{i=1}^{N_S} v_i \iint P[Y > y^*|m, r] f_{M_i}(m) f_{R_i}(r) dmdr, \tag{2}$$

where $\sum_{n=1}^{N_S}$ is the summation of the contribution from N_sth seismogenic sources n.

PSHA uncertainties from different aspects were considered and properly treated. A logic tree approach was introduced to incorporate the uncertainties for seismogenic sources, the corresponding parameters of each source, and the GMPEs. The treatment of the weighting for each parameter is discussed in subsequent sections.

Seismic Activity Models

For the implementation of PSHA, the corresponding seismicity rate as a function of magnitude for each seismogenic source should be introduced (Eq. 2). Generally, there are two models that present the relationships, the truncated exponential model and the characteristic earthquake model. In the following, both of these models are presented and discussed.

The Truncated Exponential Model

The truncated exponential model is based on Gutenberg-Richter's Law (G-R Law) (Gutenberg and Richter 1954), as follows:

$$\log(\dot{N}) = a - bM \tag{3}$$

where $\dot{N}$ is the annual rate for events with magnitudes larger than or equal to M and a and b are constants with values larger than 0. Following on G-R Law, the truncated exponential model represents the rate for a

DOI 10.1007/978-3-642-36197-5_100-1

magnitude larger than the maximum magnitude, m_u, as 0. Thus, the cumulative annual rate, $\dot{N}(m)$, for a magnitude larger than or equal to m can be presented, as follows:

$$\dot{N}(m) = \dot{N}(m_0)\frac{\exp(-\beta(m-m_0)) - \exp(-\beta(m_u-m_0))}{1.0 - \exp(-\beta(m_u-m_0))} \quad \text{for} \quad m_u \geq m \geq m_0 \tag{4}$$

where $\dot{N}(m_0)$ represents the cumulative annual rate for a magnitude of a minimum magnitude, m_0, and m_0 and m_u represent the minimum and maximum magnitudes, respectively, of the seismogenic source. β can be represented as follows:

$$\beta = b \cdot \ln(10) \tag{5}$$

where b is the b-value in G-R Law (Eq. 3).

Wesnousky (1994) concluded that this model is suitable for regions with complex tectonic settings or multiple active faults. Thus, it was applied for shallow regional sources, deep regional sources, and subduction intraslab sources.

The Characteristic Earthquake Model

The characteristic earthquake model was first proposed by Youngs and Coppersmith (1985). In addition to earthquake parameters, the model represents the seismicity rate by incorporating geological and geomorphological information. The cumulative annual rate for a magnitude larger or equal to m can be represented as follows:

$$\begin{aligned}\dot{N}(m) &= \dot{N}^e\frac{\exp(-\beta(m-m_0)) - \exp(-\beta(m_u-1/2-m_0))}{1.0 - \exp(-\beta(m_u-1/2-m_0))} + \dot{N}^c \quad \text{for} \quad m_0 \leq m \\ &\leq m_u - \frac{1}{2}; \quad \dot{N}(m) = \dot{N}^c\frac{m_u - m}{1/2} \quad \text{for} \; m_u - \frac{1}{2} \leq m \leq m_u,\end{aligned} \tag{6}$$

where $\dot{N}^e$ and $\dot{N}^c$ represent the cumulative annual rates predicted by the truncated exponential and the characteristic earthquake models, respectively. $\dot{N}^e$ can be presented, as follows:

$$\dot{N}^e = \frac{\mu A_f S \cdot (1 - \exp(-\beta(m_u - m_0 - 1/2)))}{\exp(-\beta(m_u - m_0 - 1/2)) \cdot M_0(m_u) \cdot \left[\frac{b \cdot 10^{-c/2}}{(c-b)} + \frac{b\exp(\beta)\left(1 - 10^{-c/2}\right)}{c}\right]}, \tag{7}$$

where μ is the rigidity shear modulus, generally assumed to be 3×10^{10} Pascal (N/m^2); A_f is the fault area; S is the slip rate; and c and d are constants. $\dot{N}^c$ can be represented as follows:

$$\dot{N}^c = \frac{1}{2}\dot{N}^e\frac{b\ln 10 \cdot \exp(-\beta(m_u - 3/2 - m_0))}{(1 - \exp(m_u - 1/2 - m_0))}. \tag{8}$$

In a comparison with the truncated exponential model, the characteristic earthquake model predicted lower rates for smaller magnitudes, whereas higher rates were predicted for larger magnitudes (Youngs and Coppersmith 1985).

Encyclopedia of Earthquake Engineering
DOI 10.1007/978-3-642-36197-5_100-1

To implement the characteristic earthquake model for PSHA, the cumulative annual rate should be in form of the rate $\lambda_n(m_i)$ (Eq. 2) between the magnitude bins of $m_i \pm dm/2$, which can be represented as follows:

$$\lambda_n(m_i) = N(m_i - dm/2) - N(m_i + dm/2), \tag{9}$$

where dm is the magnitude interval for the model and $N(m_i)$ is the rate for a magnitude larger or equal to m_i.

A few previous studies (Youngs and Coppersmith 1985; Wesnousky 1994) have suggested that the behavior of seismic activity along crustal active faults and subduction interfaces follows this model. Therefore, it was applied to the two seismogenic sources.

Seismogenic Tectonics in Taiwan

Tectonic Setting

Taiwan is located within the plate boundary between the Philippine Sea Plate and the Eurasian Plate (Fig. 1). Due to the interaction of the two plates, both subduction and collision take place in this region (see entry "► Earthquakes and Tectonics: An Observation from Taiwan"). Two subduction systems surround this region. In the offshore of northeast Taiwan, the Philippine Sea Plate subducts to the

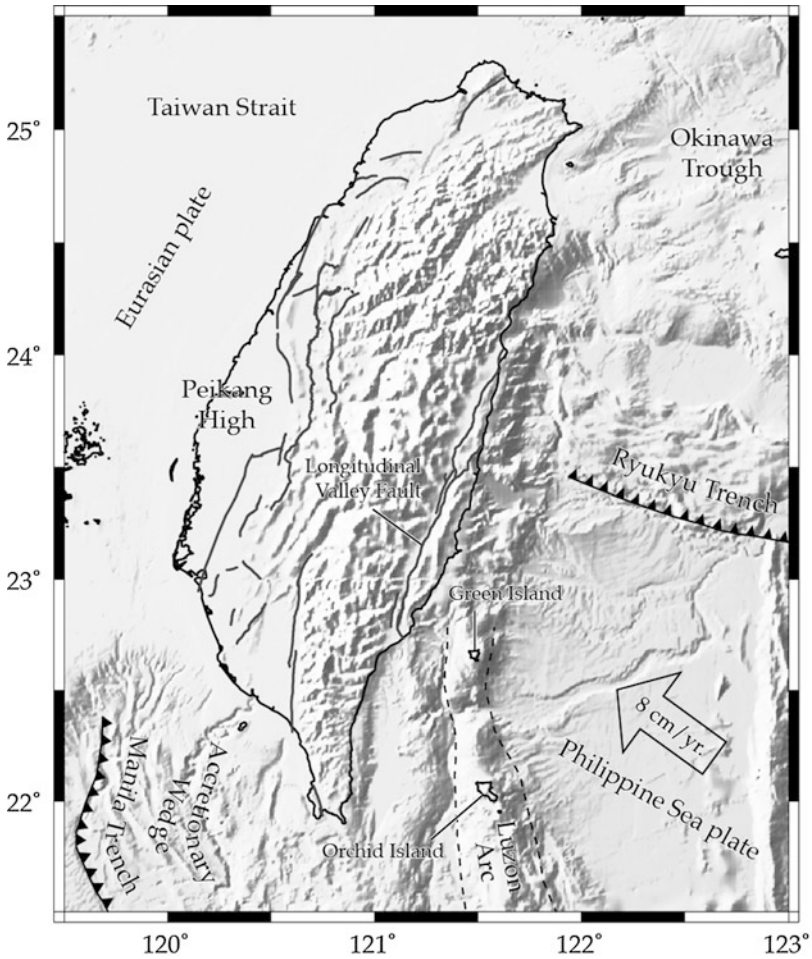

Fig. 1 The tectonic setting in Taiwan and its vicinity (Modified from Cheng et al. 2007)

DOI 10.1007/978-3-642-36197-5_100-1

north. As a result of back-arc spreading, the Okinawa Trough and the Ilan Plain formed in the northern section of the Ryukyu Volcanic Arc. In southern Taiwan, the Eurasian Plate subducts to the east. The Longitudinal Valley is the arc-continental collision boundary between the two plates. Collision began in the late Miocene in northern Taiwan. Due to lateral collision between plates, collision activity continues to migrate to the south. Currently, activity takes place in central and southwestern Taiwan. Northern Taiwan, in contrast, is a post-collision region with relatively low seismic activity.

The Earthquake Catalog

The utilized earthquake catalog was collected by the Central Weather Bureau (CWB) and provided earthquake parameters for events from 1900 to 2010 in Taiwan. Prior to 1973, a total of 15 stations equipped with Gray-Milne, Wiechert, or Omori seismographs were maintained. After 1973, the Taiwan Telemetric Seismic Network (TTSN) was established. The TTSN consists of 25 stations within the region of Taiwan. In the TTSN network, real-time signals are transmitted from field stations to a central station via leased telephone lines.

To assess seismic hazards, earthquake parameters should be analyzed using the following procedures: a magnitude harmonization from different scales, an evaluation of the magnitude of completeness, and a declustering process. In the following, each step of the procedure is described in detail.

Magnitude Harmonization

Since the magnitude scales for a catalog during different periods are generally different, it is critical to harmonize the magnitude scales during different periods. Previous studies (Hanks and Kanamori 1979 and references therein) have suggested a moment magnitude (M_W) for PSHA, since this scale is evaluated based on rupture dimensions and slip magnitudes. Additionally, the M_W scale is not affected by saturation at higher magnitudes. For example, the 1999 Chi-Chi, Taiwan, earthquake was determined to have a M_W of 7.6, whereas its corresponding M_L was 7.3. The discrepancy can be attributed to the saturation of M_L (Cheng et al. 2007). Therefore, the earthquake catalog obtained by Tsai et al. (2000) was considered. The magnitude scales of this catalog have been harmonized as M_W from 1900 to 1999. The magnitude scales of the catalog were harmonized according to the procedure of Tsai et al. (2000).

Magnitude of Completeness

To improve the reliability of the parameters for seismogenic sources, the catalog during the period when the network recorded all earthquakes with a certain magnitude threshold was considered. The threshold is known as the magnitude completeness, M_c. Thus, M_c for catalogs during different periods must be examined in advance. Chen et al. (2012) evaluated the M_c of the CWB catalog using the maximum curvature method. A higher M_c between 4.3 and 4.8 was obtained prior to 1973. Once the TTSN was established, M_c decreased to between 2.0 and 3.0. Based on the temporal distribution of M_c, $M \geq 6.0$ earthquakes after 1900 (Fig. 2) and $M \geq 2.0$ earthquakes after 1973 (Fig. 3) were considered.

The Declustering Process

For application of the PSHA approach by Cornell (1968), it is assumed that the occurrence of earthquakes follows the Poisson procedure. In other words, earthquakes are independent of one another. However, in a catalog, earthquake sequences, which include foreshocks, mainshock, aftershocks, and swarms, can be observed. Therefore, it is critical to obtain a declustered catalog in respect to the PSHA (i.e., to remove foreshocks, aftershocks, and swarms from the catalog). The declustering approaches developed by Wyss (1979), Arabasz and Robinson (1976), Gardner and Knopoff (1974), and Uhrhammer (1986) were implemented. According to these approaches, earthquakes are considered dependent when their distance

DOI 10.1007/978-3-642-36197-5_100-1

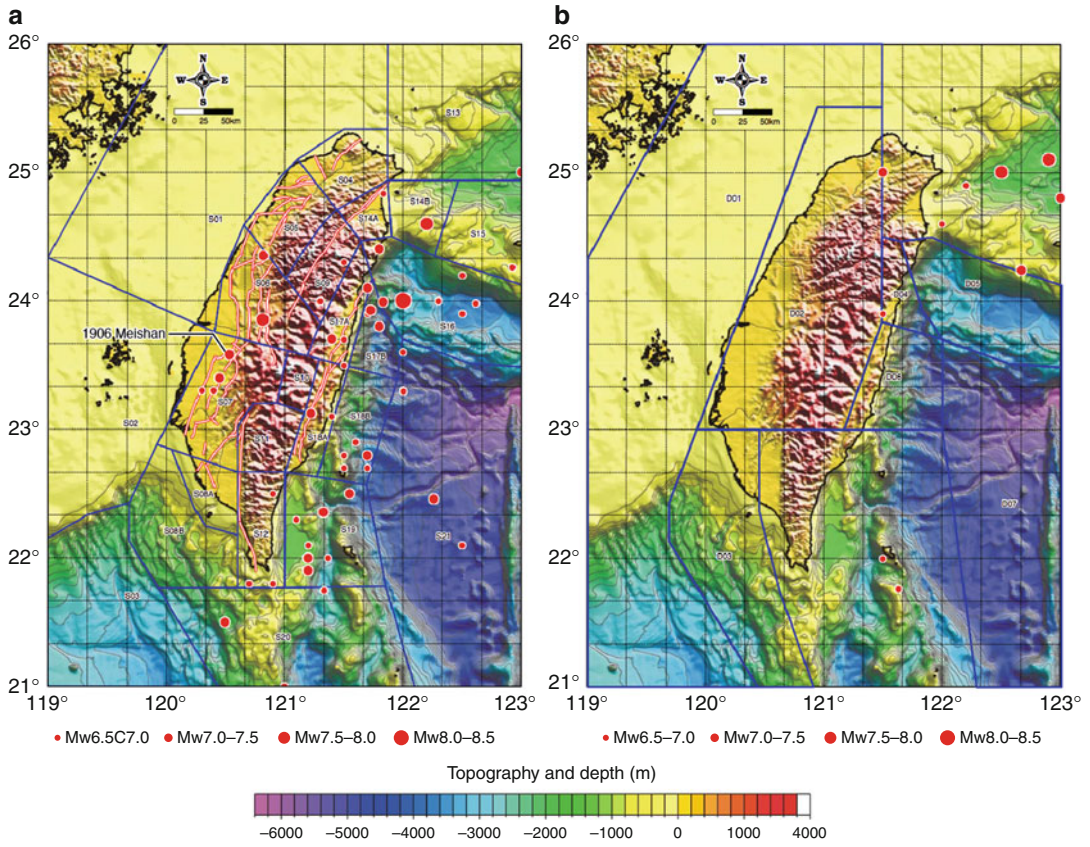

Fig. 2 The distribution of earthquakes with M ≥ 6.0 at the depth of (**a**) ≤35 km and (**b**) >35 km since 1900. The distribution of shallow and deep regional sources is illustrated by the *blue polygons* in Fig. 2a and b, respectively. In Fig. 2a, crustal active fault sources are presented as *red lines*

and time are within the windows (Fig. 4). Earthquakes are regarded as foreshocks or aftershocks if they fulfill at least two of the four declustering approaches.

Focal Mechanisms

Based on the spatial distribution of the focal mechanisms, the seismogenic region for the PSHA can be distinguished. According to the focal mechanisms determined by Wu et al. (2010), the spatial distribution of the crustal stress state in Taiwan can be illustrated. In northern Taiwan, along the Central Range and in the Okinawa Trough, the stress states are normal favorable. In central Taiwan, southwestern Taiwan, and within the interfaces of subduction systems, the stress states are thrust favorable. In northwestern Taiwan, south Taiwan, and along the Longitudinal Valley, the stresses are strike-slip favorable. Additionally, the stress state within the two subduction systems can be comprehended using focal mechanisms determined by Wu et al. (2010).

The distribution of focal mechanisms can be associated with the tectonic setting, as mentioned above (in section "Tectonic Setting"). Representing the spatial distribution of stress states in each region would be of benefit for the PSHA in respect to the determination of seismogenic sources.

Encyclopedia of Earthquake Engineering
DOI 10.1007/978-3-642-36197-5_100-1

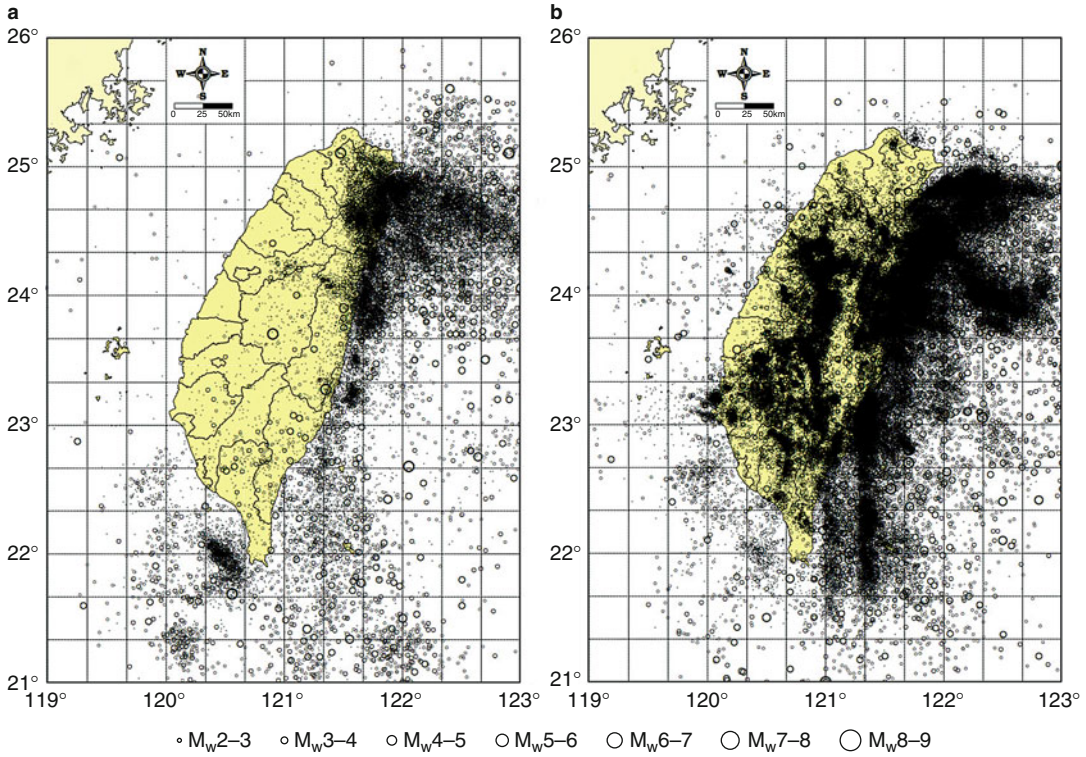

Fig. 3 The distribution of earthquakes with M $\geq$ 2.0 at a depth of (**a**) $\leq$35 km and (**b**) >35 km since 1973. In the column of rake, *N* normal, *RL* right-lateral, *LL* left-lateral, *T* thrust

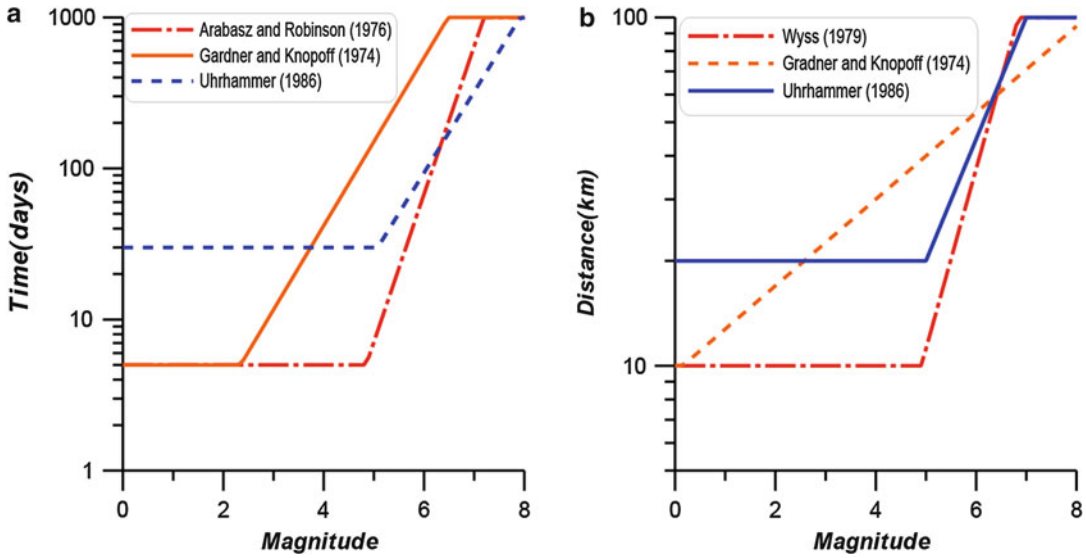

Fig. 4 The (**a**) distance and (**b**) time windows for each declustering approach. Earthquakes were considered dependent when their distance and time were within the windows

Seismogenic Sources

For application of the PSHA approach of Cornell (1968) (Eq. 2), seismogenic sources and corresponding parameters should be defined. Based on the understanding of each source, three types, Type I, Type II, and

DOI 10.1007/978-3-642-36197-5_100-1

Type III (Kiureghian and Ang 1977), can be categorized. Type I is a source with a clear fault geometry, Type II is a source with a clear focal mechanism, and Type III is a source with a controversial fault geometry and mechanism. Type II sources were assumed as "regional sources." By further considering the depth boundary of 35 km, a "shallow regional source" and a "deep regional source" were defined. Type I sources were treated as "crustal active fault sources" according to the distribution of active faults obtained by the Central Geological Survey (2010, http://fault.moeacgs.gov.tw/TaiwanFaults_2009/News/NewsView.aspx?id=3). Since two subduction systems exist in Taiwan (Fig. 1) and since the ground motion attenuation behaviors of intraslab and interface events are different, "subduction intraslab sources" and "subduction interface sources" were considered. In the following, each seismogenic source and the corresponding parameters are described in detail. For application of the logic tree in the PSHA, the weights for the parameters of each source are also required. In the following, the treatment of the weighting is described in detail.

Shallow Regional Sources

Using information on geomorphology, seismology, and geophysics, 28 shallow regional sources were defined in Taiwan and its vicinity (Fig. 5). The geometry and the corresponding parameters of each zone are outlined in the following sections.

The Geometry of Each Source

S01, S02, and S03 are located in the stable Eurasian Continental Plate. In these sources, seismicity rates are relatively low in comparison to the region surrounding Taiwan Island. The boundary between S01 and S02 was determined based on the extended alignment of the structure in Taiwan. Additionally, earthquakes for the two sources present different focal mechanisms (Wu et al. 2010). The southern boundary of S02 is defined by the accretionary wedge of the southern subduction zone system. The eastern boundary of S03 is defined by the southern subduction zone system (Fig. 1).

At S04, the focal mechanisms suggest normal favorability, which is significantly different from that in its vicinity (Wu et al. 2010). S05A displays a transient mechanism from the normal mechanism in the northeast (S04) to the strike-slip and one located in the southwest (S05B). The eastern boundary of the two sources is defined based on different mechanisms from S09, where the dipping angles of earthquakes are close to vertical and mechanisms are normal favorable. S06 belongs to the frontal deformation region in the Western Foothills. Both the southern and northern boundaries are defined by fault segmentations and changes in the fault alignments (Fig. 2a). The western boundary is marked by the boarder of the Peikang High (Fig. 1). The eastern boundary is defined due to different mechanisms from S10, where the dipping angles are close to vertical and earthquakes are the normal favorable mechanism.

S07 is also located in the frontal deformation region within the Western Foothills. The eastern boundary is defined according to a significantly different seismicity rate from S11. S08A and S08B are located in the transition region between the frontal deformation region on the north and the subduction system on the south. In comparison with the thrust mechanisms in S07, earthquakes within S08A are strike-slip types with a thrust component. The eastern boundary with S12 was determined according to heterogeneous deformation behaviors obtained from GPS observations (Hsu et al. 2009).

S09, S10, S11, and S12 are located within the transition region from the frontal deformation region in the west to the collision boundary between the Eurasian and Philippine Sea Plates in the east. The principal stress axis is vertical. The four sources are distinguished by strike orientations (from a NE-SW orientation in the north to a N-S orientation in the south) and seismicity rates. S13's source is located within the western flank of the Okinawa Trough. Due to back-arc spreading, the mechanism of earthquakes in this source suggests normal favorability. S14A, S14B, and S14C result from back-arc spreading and subduction. In the three sources, the seismicity rates are high and the seismicity behaviors are

Encyclopedia of Earthquake Engineering
DOI 10.1007/978-3-642-36197-5_100-1

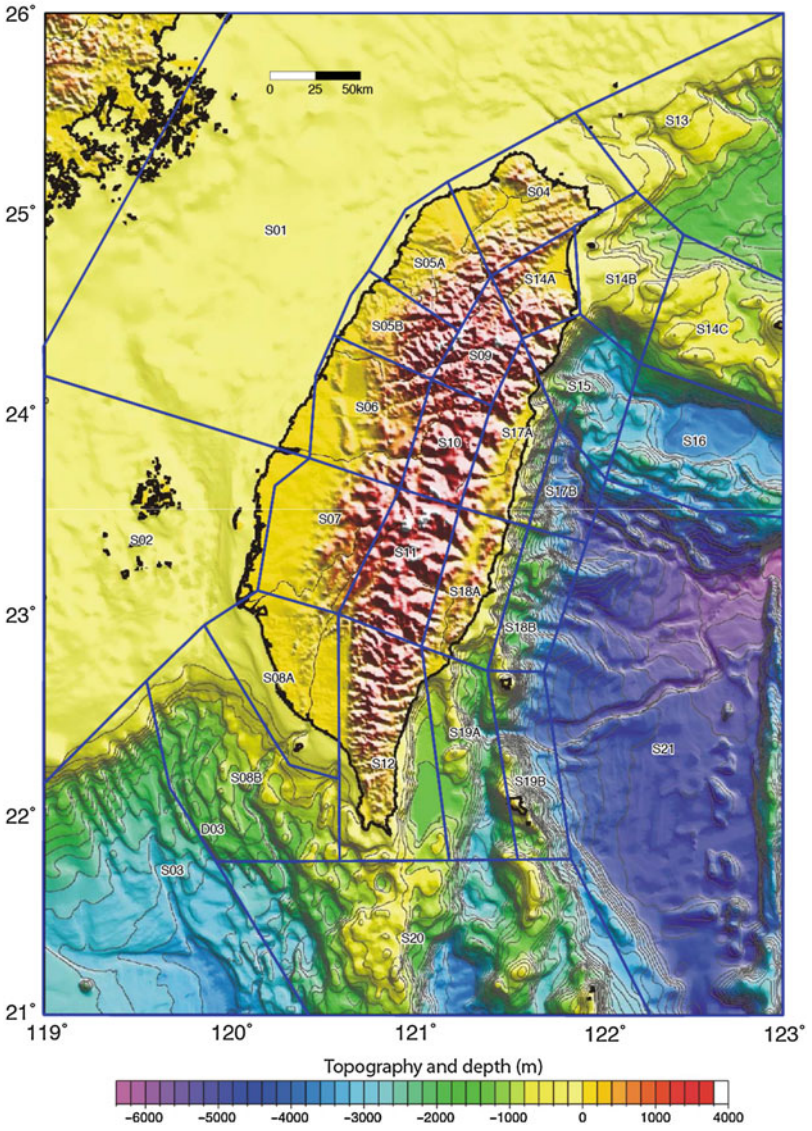

Fig. 5 The distribution of shallow regional sources

complex. The southern boundary is defined according to the interface of the subduction system. The three sources are distinguished by their seismicity rates and mechanisms. S15 and S16 are located in the area where the Philippine Sea Plate subducts to the Eurasian Plate. In general, earthquakes have thrust mechanisms with low dipping angles. In comparison, the mechanisms in S15 are complex due to the coexistence of plate collision and subduction. For the same reason, the seismicity rate in S15 is higher than that in S16.

S17A, S17B, S18A, and S18B reside along the eastern coastline and in the offshore region, which is in the collision zone between the two plates. The boundary between S17 and S18 is defined by heterogeneities in respect to active fault activity and deformation behavior according to GPS observations (Hsu et al. 2009). Additionally, seismicity rates in S17A and S18A to the west are higher than those in S17B and S18B to the east. Earthquakes in these sources are mainly thrusts with a strike-slip mechanism with high dipping angles.

S19A and S19B include Green Island and Orchid Island and their vicinity. Since 1900, eight earthquakes with $M \geq 6.0$ have taken place in these sources (Fig. 2a). The two sources are distinguished based

DOI 10.1007/978-3-642-36197-5_100-1

on differences in the seismicity rate (Fig. 3a). S20 represents the southern offshore region of Taiwan. Additionally, it is above the subduction zone. S21 is located within the Philippine Sea Plate. Since it is located at a distance from the collision zone, the seismicity rate is relatively low (Fig. 1).

The Parameters of Each Source

In the above discussion, the distributions of shallow regional sources were determined. For application of the PSHA, parameters for each source were required. In the following, the acquirement of parameters including the seismicity rate models, maximum magnitudes, and their corresponding weights is described.

Due to insufficient information on fault geometry and the slip rate for regional sources, a truncated exponential model (Eq. 4) is applied for shallow regional sources. The model for each source was obtained through a regression of the declustered catalog using maximum likelihood estimates. For the regression, the magnitude interval for the model (dm in Eq. 7) was assumed to be 0.5. Therefore, the cumulative annual rate ($\dot{N}(m_0)$) and the b-value, as well as the corresponding deviations for each source, were obtained (Table 1).

Table 1 The parameters and the corresponding standard deviations for the 28 shallow regional sources; the corresponding weights for the maximum magnitudes, m_u, are denoted in parentheses

NO	m_0	$\mathrm{N}(m_0)\left(\pm\sigma_{N(m_0)}\right)$	$b(\pm\sigma_b)$	m_u
S01	3.5	1.108(±0.171)	0.865(±0.114)	6.5(0.2) 6.6(0.6) 6.7(0.2)
S02	3.5	0.968(±0.159)	0.772(±0.114)	6.5(0.2) 6.6(0.6) 6.7(0.2)
S03	3.5	0.806(±0.185)	0.852(±0.162)	6.5(0.2) 6.6(0.6) 6.7(0.2)
S04	2.5	3.578(±0.384)	0.783(±0.066)	6.5(1.0)
S05A	2.5	4.498(±0.349)	1.194(±0.093)	5.5(1.0)
S05B	2.5	5.412(±0.382)	0.811(±0.053)	6.5(1.0)
S06	2.5	11.860(±0.702)	0.816(±0.041)	6.5(1.0)
S07	3	6.107(±0.400)	0.643(±0.034)	6.5(1.0)
S08A	2.5	9.990(±0.649)	0.855(±0.049)	6.5(1.0)
S08B	2.5	14.280(±0.852)	1.028(±0.051)	6.5(0.2) 6.6(0.6) 6.7(0.2)
S09	2.5	1.925(±0.269)	0.0541(±0.062)	6.7(0.2) 6.9(0.6) 7.1(0.2)
S10	3.5	0.935(±0.157)	0.958(±0.136)	6.5(0.2) 6.7(0.6) 6.9(0.2)
S11	3.5	1.543(±0.201)	0.857(±0.094)	6.5(1.0)
S12	2.5	23.510(±0.966)	0.695(±0.024)	7.0(1.0)
S13	3	5.185(±0.497)	0.692(±0.049)	6.3(0.2) 6.5(0.6) 6.7(0.2)
S14A	2.5	3.526(±0.373)	0.676(±0.058)	6.7(0.2) 6.9(0.6) 7.1(0.2)
S14B	2.5	1.523(±0.198)	0.564(±0.061)	7.4(0.2) 7.6(0.6) 7.8(0.2)
S14C	3.5	4.013(±0.326)	0.720(±0.048)	7.4(0.2) 7.6(0.6) 7.8(0.2)
S15	3.5	7.187(±0.528)	0.629(±0.037)	7.0(1.0)
S16	3.5	6.285(±0.0.491)	0.602(±0.036)	7.0(1.0)
S17A	3.5	4.069(±0.405)	0.713(±0.055)	6.5(1.0)
S17B	3.5	1.795(±0.268)	0.685(±0.081)	7.3(0.2) 7.5(0.6) 7.7(0.2)
S18A	3.5	2.979(±0.274)	0.616(±0.048)	6.5(1.0)
S18B	3.5	2.524(±0.253)	0.636(±0.054)	7.3(0.2) 7.5(0.6) 7.7(0.2)
S19A	3.5	4.834(±0.438)	0.678(±0.049)	7.3(0.2) 7.5(0.6) 7.7(0.3)
S19B	3.5	3.017(±0.353)	0.780(±0.071)	7.3(0.2) 7.5(0.6) 7.7(0.3)
S20	3.5	4.866(±0.456)	0.882(±0.064)	7.1(0.2) 7.3(0.6) 7.5(0.2)
S21	3.5	9.581(±0.498)	0.756(±0.033)	7.1(0.2) 7.3(0.6) 7.5(0.2)

DOI 10.1007/978-3-642-36197-5_100-1

Another key parameter for the PSHA was the maximum magnitude, m_u. For sources with active faults or subduction systems (i.e., S04, S05A, S05B, S06, S07, S08A, S11, S12, S15, S16, S17A, and S18A) (Fig. 2a), the corresponding m_u's were generally obtained based on the maximum magnitude of active faults within the source (see section "Crustal Active Fault Sources"). Note that a maximum threshold of 6.5 in these sources was assumed since the occurrence of $M > 6.5$ earthquakes can be attributed to crustal active faults or subduction sources. However, m_u for some sources, S05A, S12, S15, and S16, was determined using other considerations. In S05A, since no earthquake with $M \geq 5.0$ has ever been recorded, a smaller m_u of 5.5 was assumed. In S12, S15, and S16, due to the existence of a subduction interface and other offshore active faults, a larger m_u of 7.0 was assumed. On the other hand, for sources without active faults (i.e., S01, S02, S03, S08B, S09, S10, S13, S14A, S14B, S14C, S17B, S18B, S19A, S19B, S20, and S21), the m_u's were assumed based on the maximum observed earthquake plus 0.2 for each source (Table 1).

Deep Regional Sources

According to the distribution of seismicity and the tectonic setting, seven deep regional sources were defined in Taiwan and its vicinity (Fig. 6). Note that subduction interfaces were not included with respect to differences in ground motion attenuation behaviors (Lin and Lee 2008). The geometry and the corresponding parameters of each source are discussed in the following sections.

The Geometry of Each Source

Deep regional sources can be separated into two parts. To the east of longitude 121.5°, they are located within the subduction zone in northeast Taiwan. To the south of latitude 23°, they are regarded as another subduction zone in southern Taiwan. D01, D02, and D03 are located within the Eurasian Plate. The boundary between D02 and D03 is located along the latitude of 23°, which is regarded as the border of the continent to the north and the subduction zone to the south. The accretionary wedge of the southern subduction zone system defines the western boundary of D03. The eastern boundary of D03 is illustrated by the distribution of the southern subduction zone system. To the east of Taiwan, four deep regional sources, including D04, D05, D06, and D07, were identified. Due to plate collision, higher seismicity rates were observed in D04 and D06 (Fig. 3b). In contrast, since it is a part of the deeper part of the Philippine Sea Plate, D07 has a lower seismicity rate. D05 is located within the region where the Philippine Sea Plate subducts to the Eurasian Plate.

The Parameters of Each Source

As a follow-up to the procedure for shallow regional sources, the acquirement of the corresponding parameters for each deep regional source is described in the following. A truncated exponential model is used to present seismic activity. The cumulative annual rate and the b-value, as well as the corresponding deviations for each source, were obtained (Table 2). The maximum magnitude, m_u, for each source was assumed. Since D01, D02, and D03 are located within the stable Eurasian Continental Plate, a small m_u was assumed. For application of the logic tree, weights of 0.2, 0.6, and 0.2 were assumed for m_u's of 6.5, 6.6, and 6.7, respectively. Due to the plate collision zone, higher m_u's of 7.0, 7.2, and 7.4 were assumed for D04. Since earthquakes with $M \geq 6.7$ have never been recorded in D05, D06, and D07, m_u's of 6.8, 7.0, and 7.2 were assumed.

Crustal Active Fault Sources

Thirty-three active faults obtained by the Central Geological Survey (2010, http://fault.moeacgs.gov.tw/TaiwanFaults_2009/News/NewsView.aspx?id=3) and three blind faults by Cheng et al. (2007) were considered as crustal active fault sources (Fig. 7). Crustal active fault sources are categorized as Type

DOI 10.1007/978-3-642-36197-5_100-1

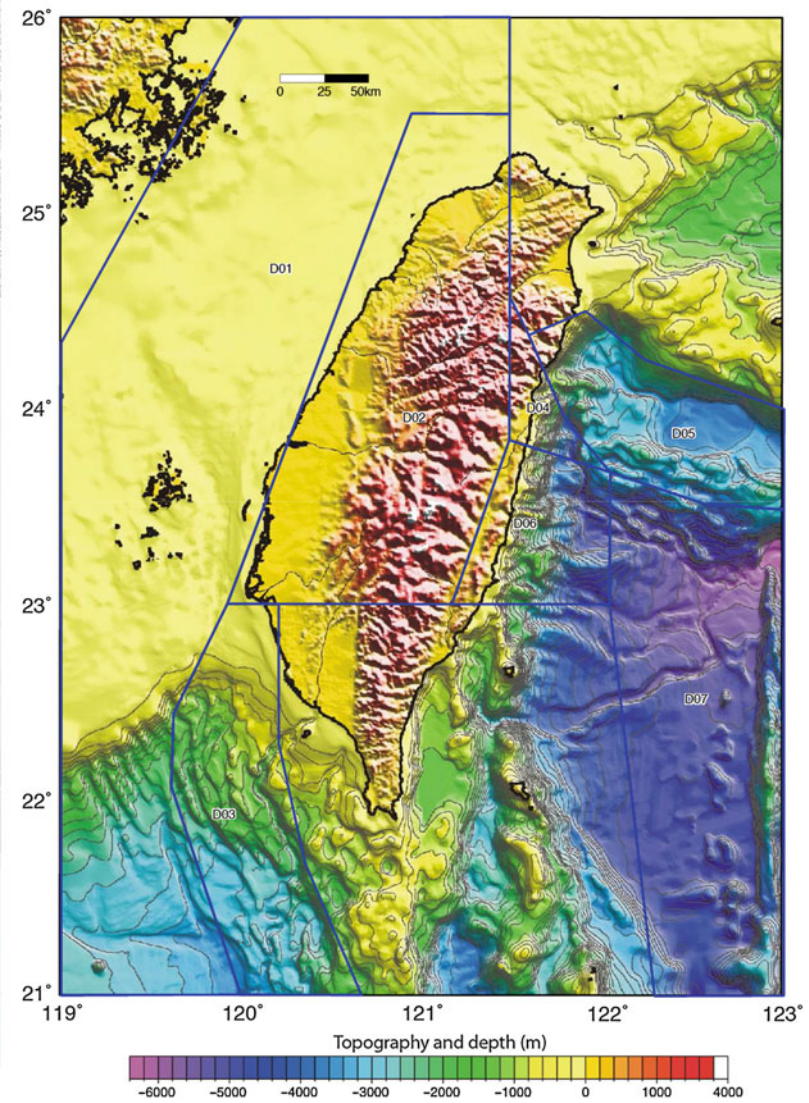

Fig. 6 The distribution of deep regional sources

Table 2 The parameters and the corresponding standard deviations for the seven deep regional sources; the corresponding weights of the maximum magnitudes, m_u, are denoted in parentheses

NO	m_0	$\mathrm{N}(m_0)\,(\pm\sigma_{N(m_0)})$	$b(\pm\sigma_b)$	m_u
D01	3.5	0.673(±0.169)	0.837(±0.162)	6.5(0.2) 6.6(0.6) 6.7(0.2)
D02	3.0	2.142(±0.239)	0.799(±0.078)	6.5(0.2) 6.6(0.6) 6.7(0.2)
D03	3.0	7.341(±0.596)	0.750(±0.055)	6.5(0.2) 6.6(0.6) 6.7(0.2)
D04	3.5	1.340(±0.185)	0.668(±0.077)	7.0(0.2) 7.2(0.6) 7.4(0.2)
D05	3.5	3.394(±0.299)	0.669(±0.052)	6.8(0.2) 7.0(0.6) 7.2(0.2)
D06	3.5	1.585(±0.204)	0.665(±0.072)	6.8(0.2) 7.0(0.6) 7.2(0.2)
D07	3.5	1.374(±0.185)	0.554(±0.070)	6.8(0.2) 7.0(0.6) 7.2(0.2)

I sources by Kiureghian and Ang (1977). Sources of this type usually generate earthquakes with a characteristic magnitude repeatedly within a recurrence interval. Such seismic activity does not follow the truncated exponential model, but fulfills the characteristic earthquake model (Wesnousky 1994). For

Encyclopedia of Earthquake Engineering
DOI 10.1007/978-3-642-36197-5_100-1

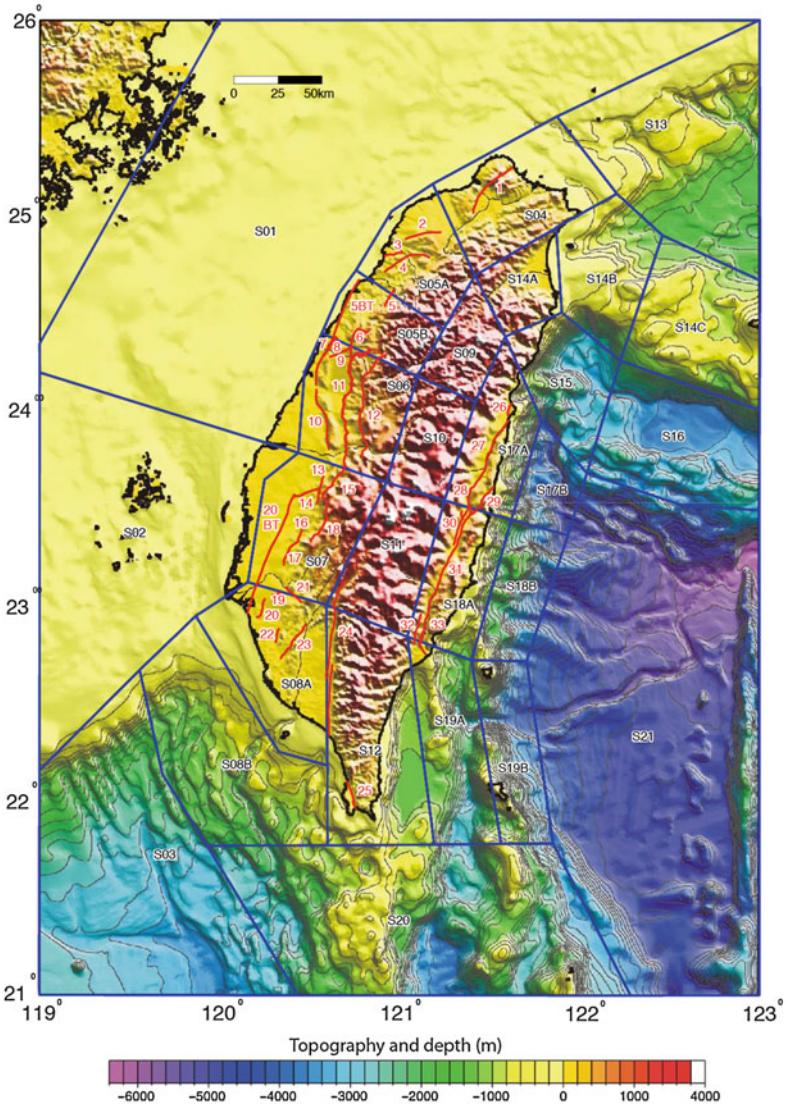

Fig. 7 The distribution of shallow regional (*blue polygons*) and crustal active fault sources (*red lines*). The corresponding shallow regional source and the *b*-values for each crustal active fault source are denoted in Table 4

application of this model, some parameters are required (Eqs. 6, 7, and 8). The fault parameters, including segmentation, length, depth, area, the rupture mechanism, dip angle, the possible magnitude of the slip, the slip rate, the recurrence interval, the last slip time, and the magnitude of a characteristic event, were obtained from various references and are listed in Table 3. For treatment of the *b*-value, a constant *b*-value is assumed in each shallow regional source. According to the distribution of shallow regional sources and crustal active fault sources (Fig. 7), the corresponding *b*-value for each source was obtained. Table 4 summarizes the *b*-value for crustal active fault sources.

Subduction Interface Sources

Typical interface sources take place along plate boundaries within subduction zones. Two subduction systems are located within the vicinity of Taiwan (Fig. 1). Subduction interface sources exist in both systems (Fig. 8). In the northeast subduction system, an interface earthquake with M8.2 took place in 1920 (Tsai et al. 2000) and is the largest earthquake ever recorded in T01A. m_u's of 8.0, 8.2, and 8.4 with corresponding weights of 0.2, 0.6, and 0.2 were assumed for this source. The interface in the southern

Table 3 The parameters for crustal active fault sources; the corresponding weights of the slip rate and the maximum magnitude for each source are denoted in parentheses

ID	Length (km)	Depth (km) Top	Bottom	Area (km2)	Rake	Dip angle	Possible slip amount (m)	Slip rate (mm/year)	Recurrence interval (year)	Last occurrence time (year)	Characteristic magnitude(Mw)
1	61	0	15	1,009.6	N	>60°E	1.39 ~ 7.99	0.69(1)	614 ~ 2,511	<11,000	7.20(0.5) 7.33(0.5)
	13	0	15	215.2	N	>60°E	0.23 ~ 1.30	1.2(0.5) 18(0.5)			
2	22	0	12	410.7	T	~40°S	0.46 ~ 3.20	0.9(0.2) 1.7(0.6) 2.5(0.2)	117 ~ 527	<70,000	6.50(0.5) 6.64(0.5)
3	9	0	12	141	T-RL	~50°S	0.34 ~ 2.33	1.0(0.5) 1.2(0.5)	118 ~ 263	Late Pleistocene	5.98(0.5) 6.16(0.5)
4	28	0	12	672	T	~30°S	0.50 ~ 3.48	1.0(0.5) 1.6(0.5)	181 ~ 454	<300 year	6.64(0.5) 6.77(0.5)
5	12	0	12	158.8	T	>60°W	0.37 ~ 2.58	1.3(0.2) 2.5(0.6) 3.8(0.2)	60 ~ 314	A.D.1935	6.15(0.5) 6.32(0.5)
5BT	37	2	15	962	T-RL	30°E	0.56 ~ 3.84	2.5(0.2) 5.0(0.6) 7.5(0.2)	47 ~ 207		6.80(0.5) 6.91(0.5)
6	33	0	15	646.2	T	40–60°E	0.53 ~ 3.69	0.5(0.2) 1.0(0.6) 1.5(0.2)	275 ~ 1,249	Holocene	6.73(0.5) 6.85(0.5)
7	8	2	15	147.1	T	40–50°E	0.46 ~ 3.20	1.7(0.2) 3.6(0.6) 5.5(0.2)	74 ~ 362	Holocene	6.68(0.5) 6.80(0.5)
	22	2	15	404.4		40–50°E	0.32 ~ 2.24				
8	13	2	15	399.9	T	20–30°W	0.38 ~ 2.66	1.2(1)	86 ~ 155	Holocene	6.19(0.5) 6.36(0.5)
9	14	0	15	210	RL	High angle	0.17 ~ 0.79	1.3(0.2) 2.5(0.6) 3.8(0.2)	59 ~ 312	A.D.1935	6.23(0.5) 6.4(0.5)
10	36	2	15	936	T	18–45°E	0.55 ~ 3.81	4.3(0.2) 7.3(0.6) 103(0.2)	33 ~ 119	Holocene	6.78(0.5) 6.9(0.5)
11	36	0	20	1,120.1	T	~40°E	0.55 ~ 3.81	3.5(0.5) 6.9(0.5)	112 ~ 280	A.D.1999	7.36(0.5) 7.43(0.5)
	48	0	20	1,493.5			0.61 ~ 4.22				
	14	0	20	435.6			0.39 ~ 2.73				
12	69	0	15	1,463.7	T	~45°E	0.69 ~ 4.79	0.4(0.2) 0.8(0.6) 1.2(0.2)	670 ~ 2,651	A.D.1999	7.16(0.5) 7.24(0.5)
13	17	0	15	603.4	T	20–30°E	0.42 ~ 2.92	5(0.2) 10(0.6) 15(0.2)	8 ~ 40	<18,540 BP	6.35(05) 6.6(0.5)
14	13	0	15	215.2	RL	>60°	0.15 ~ 0.72	3(0.2) 6(0.6) 9(0.2)	22 ~ 117	A.D.1906	6.19(0.5) 6.36(0.5)
14BT	36	2	15	936	T	30°E	0.55 ~ 3.81	6(0.2) 12(0.6) 18(0.2)	19 ~ 87		6.78(0.5) 6.90(0.5)
15	25	0	15	433	T-RL	>60°E	0.48 ~ 3.25	5(0.2) 10(0.6) 15(0.2)	24 ~ 116	A.D.1999	6.57(0.5) 6.71(0.5)
16	7	0	15	154	T	~30°E	0.31 ~ 2.13	8.2(0.5) 9.3(0.5)	8 ~ 19	Late Pleistocene	5.83(0.5) 6.03(0.5)
17	17	0	15	373.9	T-LL	~30°E	0.42 ~ 2.92	8.2(0.5) 9.3(0.5)	21 ~ 40	<10,000	6.35(0.5) 6.50(0.5)
18	28	0	15	512.7	T	50–60°E	0.50 ~ 3.48	5(0.2) 10(0.6) 15(0.2)	26 ~ 121	<10,000	6.64(0.5) 6.77(0.5)
19	6	0	15	99.3	RL	>60	0.06 ~ 0.27	2.5(0.2) 5(0.6) 7.5(0.2)	12 ~ 72	A.D.1946	5.74(0.5) 5.95(0.5)

20	12	0	15	280	T	>35°W	0.37 ~ 2.58	4.0(0.5) 5.6(0.5)	23 ~ 58	Late Pleistocene	6.15(0.5) 6.32(0.5)
20BT	36	2	15	936	T	30°E	0.55 ~ 3.81	5(0.2) 10(0.6) 15(0.2)	23 ~ 104		6.78(0.5) 6.90(0.5)
21	10	0	15	165.5	LL	>60°N	0.11 ~ 3.81	1.3(0.2) 2.5(0.6) 3.8(0.2)	40 ~ 216	Mid-late Pleistocene	6.04(0.5) 622(0.5)
22	8	0	15	169.7	T	45°E	0.32 ~ 2.24	4.0(0.5) 5.6(0.5)	15 ~ 40	Mid-late Pleistocene	5.91(0.5) 6.10(0.5)
23	30	0	15	587.4	T	High angle	0.52 ~ 3.57	15(0.2) 3(0.6) 4.5(0.2)	85 ~ 385	7,189 BP	6.68(0.5) 6.80(0.5)
24	28	0	20	579.8	T-LL	70–80°E	0.50 ~ 3.48	2(0.2) 4(0.6) 6(0.2)	57 ~ 266	Late Pleistocene	6.64(0.5) 6.77(0.5)
	61			1,263			0.66 ~ 4.59	1.5(0.2) 3(0.6) 4.5(0.2)	26 ~ 122		7.09(05) 7.18(0.5)
25	39	0	20	830.1	T	70°E	0.57 ~ 3.92	4.2(0.5) 7.5(0.5)	61 ~ 159	Late Pleistocene	6.83(0.5) 6.94(0.5)
26	8	0	30	264.8	LL-T	60–70°E	0.32 ~ 2.24	10(0.2) 20(0.6) 30(0.2)	2 ~ 12	A.D.1951	5.91(0.5) 6.10(0.5)
27	30	0	30	1,174.9	LL-T	50°E	0.52 ~ 3.57	10(0.2) 20(0.6) 30(0.2)	6 ~ 29	Late Pleistocene	6.68(0.5) 6.80(0.5)
28	33	0	30	1,292.3	T-LL	40–50°E	0.53 ~ 3.69	12.5(0.5) 16.0(0.5)	13 ~ 25	A.D.1951	6.73(0.5) 6.85(0.5)
29	30	0	30	931.7	T	E	0.52 ~ 3.57	2(0.2) 4(0.6) 6(0.2)	40 ~ 183	Late Pleistocene	6.68(0.5) 680(0.5)
30	23	0	25	750.6	LL-T		0.47 ~ 3.25	8(0.2) 16(0.6) 24(0.2)	7 ~ 35	A.D.1951	6.52(0.5) 6.66(0.5)
31	67	0	30	2,217.8	T-LL	~65°E	0.69 ~ 4.74	26(0.5) 30(0.5)	17 ~ 26	A.D.2003	7.14(0.5) 7.23(0.5)
32	17	0	25	554.8	T	50°E	0.42 ~ 2.92	1.9(0.5) 3.0(0.5) 5.4(0.5) 5.5(0.5)	24 ~ 116	Late Pleistocene	6.35(0.5) 6.50(0.5)
33	20	0	25	551.7	T	65°E	0.45 ~ 3.09	8(0.2) 16(0.6) 24(0.2)	8 ~ 38	Late Pleistocene	6.44(05) 6.59(0.5)

DOI 10.1007/978-3-642-36197-5_100-1

Table 4 The corresponding shallow regional source and *b*-values for each crustal active fault source; the spatial distribution of the sources is presented in Fig. 7

Shallow regional sources	*b*-value	Active fault sources (ID)
S04	0.783	1
S05A	1.194	2, 3, 4,
S05B	0.811	5, 5BT, 6
S06	0.816	7, 8, 9, 10, 11, 12
S07	0.643	13, 14, 14BT, 15, 16, 17, 18, 20BT, 21
S08A	0.855	19, 20, 22, 23
S12	0.695	24, 25
S17A	0.713	26, 27, 28, 29
S18A	0.616	30, 31, 32, 33

subduction system was defined according to the profiles of earthquake distribution. Three interface sources, T02A, T02B, and T02C, were defined (Fig. 8). Segmentations were defined by the bending of the accretionary wedge. Parameters for subduction interface sources are summarized and presented in Table 5. The characteristic earthquake model provides the behaviors of the seismic activity for the sources.

Subduction Intraslab Sources

The geometries of intraslab sources for subduction systems are illustrated based on the profiles of the earthquake distribution. Ten and three interface sources were defined for the northeastern and southern subduction zones, respectively (Fig. 8). Seismic activities of the sources were determined using the truncated exponential model. The corresponding m_u's were inferred from the maximum magnitudes of the intraslab earthquakes surrounding Taiwan and the world. The parameters and the corresponding weights for subduction intraslab sources are summarized and presented in Table 6.

Ground Motion Prediction Equations (GMPEs)

For the application of the PSHA, in addition to reliable seismogenic sources, another key factor is proper GMPEs (Encyclopedia of Earthquake Engineering: Ground Motion Prediction Equations). Lin (2009) pointed out that global GMPEs do not truly represent ground motion attenuation behaviors in Taiwan. Thus, only GMPEs obtained from the regression of strong ground motion observations in Taiwan were considered. Several studies have proposed GMPEs in order to model the attenuation behaviors for different types of earthquakes in Taiwan. For a more complete presence of attenuation behaviors, GMPEs with the form of an acceleration response spectrum (SA) are expected. In the form of SA, attenuation behaviors are presented as a response acceleration as a function of the response period. Lin (2009) considered 5,968 observations of 60 crustal earthquakes recorded by the Taiwan Strong Motion Instrumentation Program (TSMIP). GMPEs as a function of magnitude, m, are determined as follows:

$$\ln y = C_1 + F_1 + C_3(8.5 - m)^2 + (C_4 + C_5(m - 6.3))\ln\left(\sqrt{R^2 + \exp(H)^2}\right) + C_6 F_{NM} + C_7 F_{RV} + C_8 \ln(Vs_{30}/1,130.0), \quad (10)$$

DOI 10.1007/978-3-642-36197-5_100-1

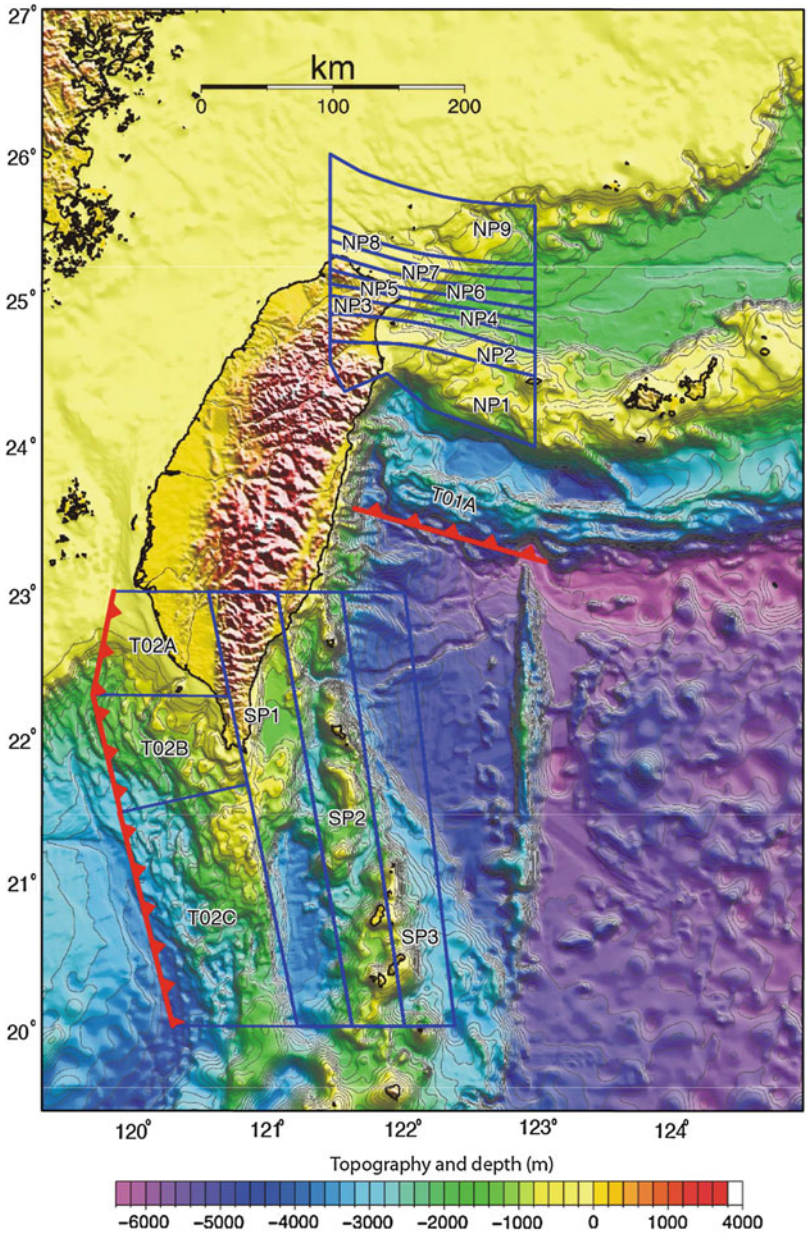

Fig. 8 The distribution of the subduction interface and the intraslab sources illustrated by *blue polygons*. The surface alignments of the two trenches are presented in *red*

where y represents the response acceleration for PGA or SA in g; R represents the shortest distance to the rupture surface in kilometers; F_{NM} is 1.0 when the sources are normal mechanisms; F_{RV} is 1.0 when the sources are thrust mechanisms; Vs_{30} represents the average shear-wave velocity from the ground surface down to a depth of 30 m; $F_1 = C_{2(M_W-6.3)}$ for $M_W \leq 6.3$, whereas $F_1 = (-H \cdot C_5)(M_W - 6.3)$ for $M_W > 6.3$; and C_1 to C_8 and H are constants. The corresponding parameters for PGA and SA are presented in Table 7. Note that through these GMPEs, source effects in the form of different focal mechanisms were considered and indicated that the largest amplitudes for thrust events and the smallest for normal ones were obtained based on the same magnitude and distance to the rupture surface. In order to present the reliability of these GMPEs, the corresponding standard deviations were analyzed and are presented as σ_{lny} in Table 8. These GMPEs were applied for crustal sources.

DOI 10.1007/978-3-642-36197-5_100-1

Table 5 The parameters for five of the subduction interface sources; the corresponding weights for the slip rate, dip angle, and maximum magnitudes, m_u, are denoted in parentheses

NO	m_0	Slip rate (mm/year)	Dip angle (°)	Depth (km)	*b*-value	m_u
T01A	6.5	20(0.2)	18(0.3)	0–40	0.6	8.0(0.2)
		30(0.6)	20(0.4)			8.2(0.6)
		40(0.2)	22(0.3)			8.4(0.2)
T02A	6.5	5(0.2)	18(0.3)	0–35	0.7	7.6(0.2)
		10(0.6)	20(0.4)			7.8(0.6)
		15(0.2)	22(0.3)			8.0(0.2)
T02B	6.5	5(0.2)	18(0.3)	0–35	0.7	7.7(0.2)
		10(0.6)	20(0.4)			7.9(0.6)
		15(0.2)	22(0.3)			8.1(0.2)
T02C	6.5	5(0.2)	18(0.3)	0–35	0.7	7.9(0.2)
		10(0.6)	20(0.4)			8.1(0.6)
		15(0.2)	22(0.3)			8.3(0.2)

Table 6 The parameters and the corresponding standard deviations for 13 of the subduction intraslab sources; the corresponding weighs of the maximum magnitudes, m_u, are denoted in parentheses

NO	m_o	$N(m_o)\left(\pm\sigma_{N(m_o)}\right)$	$b(\pm\sigma_b)$	m_u
NP1	4.0	3.735(±0.307)	0.908(±0.063)	7.5(0.2) 7.7(0.6) 7.9(0.2)
NP2	4.0	2.335(±0.247)	0.801(±0.070)	7.5(0.2) 7.7(0.6) 7.9(0.2)
NP3	4.0	1.197(±0.177)	0.866(±0.104)	7.5(0.2) 7.7(0.6) 7.9(0.2)
NP4	4.0	0.580(±0.119)	0.730(±0.124)	7.6(0.2) 7.8(0.6) 8.0(0.2)
NP5	4.0	0.210(±0.074)	0.938(±0.297)	7.6(0.2) 7.8(0.6) 8.0(0.2)
NP6	4.0	0.263(±0.083)	0.959(±0.272)	7.6(0.2) 7.8(0.6) 8.0(0.2)
NP7	4.0	0.344(±0.091)	0.730(±0.173)	7.6(0.2) 7.8(0.6) 8.0(0.2)
NP8	4.0	0.374(±0.098)	1.040(±0.237)	7.6(0.2) 7.8(0.6) 8.0(0.2)
NP9	4.0	0.913(±0.155)	0.913(±0.138)	7.6(0.2) 7.8(0.6) 8.0(0.2)
SP1	4.0	1.041(±0.165)	0.762(±0.106)	7.5(0.2) 7.7(0.6) 7.9(0.2)
SP2	4.0	2.735(±0.268)	0.831(±0.068)	7.6(0.2) 7.8(0.6) 8.0(0.2)
SP3	4.0	1.660(±0.209)	0.876(±0.090)	7.6(0.2) 7.8(0.6) 8.0(0.2)

Many studies (e.g., Chan et al. 2013a) have indicated that ground motion attenuation behaviors for subduction earthquakes are different than those for crustal earthquakes. Since two subduction systems are located within the Taiwan region, as well as its vicinity (Fig. 1), the different GMPEs for both interfaces and intraslab events are considered to apply PSHAs. Lin and Lee (2008) proposed the first GMPEs for subduction events in Taiwan. In order to establish the GMPEs, they analyzed the strong motion records of subduction earthquakes obtained using TSMIP arrays and the Strong Motion Array in Taiwan Phase I (SMARTI). The GMPEs of Lin and Lee (2008) are represented as follows:

$$\ln y = C_1 + C_2 m + C_3\left(R + C_4 e^{C_5 \cdot m}\right) + C_6 H + C_7 Z_t, \tag{11}$$

where y represents the response acceleration for PGA or SA in g, R represents the hypocentral distance in kilometers, H represents the focal depth in kilometers, Z_t represents the subduction zone earthquake type ($Z_t = 0$ for interface earthquakes, whereas $Z_t = 1$ for intraslab earthquakes), and C_1 to C_7 are constants. The parameters and their corresponding standard deviations for PGA and SA are presented in Table 8 and

DOI 10.1007/978-3-642-36197-5_100-1

Table 7 The corresponding parameters and the standard deviations (σ_{lny}) of the GMPEs for the PGA and each response period for crustal events (Eq. 8) as proposed by Lin (2009)

Period (s)	C_1	C_2	C_3	C_4	C_5	H	C_6	C_7	C_8	σ_{lny}
PGA	1.0109	0.3822	0.0000	−1.1634	0.1722	1.5184	−0.1907	0.1322	−0.4741	0.627
0.01	1.0209	0.3822	−0.0003	−1.1633	0.1722	1.5184	−0.1922	0.1314	−0.4738	0.627
0.02	1.0416	0.3822	0.0017	−1.1668	0.1722	1.5184	−0.1942	0.1311	−0.4700	0.627
0.03	1.1961	0.3822	0.0038	−1.2028	0.1722	1.5184	−0.1990	0.1314	−0.4741	0.640
0.04	1.3834	0.3822	0.0087	−1.2499	0.1722	1.5184	−0.1959	0.1362	−0.4806	0.655
0.05	1.5612	0.3822	0.0153	−1.2957	0.1722	1.5184	−0.1922	0.1417	−0.4911	0.670
0.06	1.6907	0.3822	0.0210	−1.3218	0.1722	1.5184	−0.1984	0.1500	−0.4900	0.681
0.07	1.7673	0.3822	0.0261	−1.3336	0.1722	1.5184	−0.2011	0.1557	−0.4920	0.691
0.08	1.8689	0.3822	0.0273	−1.3440	0.1722	1.5184	−0.1947	0.1627	−0.4944	0.699
0.09	1.9430	0.3822	0.0276	−1.3435	0.1722	1.5184	−0.2011	0.1589	−0.4910	0.700
0.10	2.0218	0.3822	0.0254	−1.3409	0.1722	1.5184	−0.1817	0.1607	−0.4825	0.705
0.15	2.0521	0.3822	0.0100	−1.2578	0.1722	1.5184	−0.1851	0.1212	−0.4804	0.691
0.20	2.0333	0.3822	−0.0091	−1.1769	0.1722	1.5184	−0.2265	0.0999	−0.4350	0.676
0.25	1.9887	0.3822	−0.0293	−1.1153	0.1722	1.5184	−0.2355	0.0994	−0.4101	0.679
0.30	1.8827	0.3822	−0.0459	−1.0726	0.1722	1.5184	−0.2163	0.1036	−0.4361	0.686
0.35	1.7459	0.3822	−0.0600	−1.0307	0.1722	1.5184	−0.1949	0.1029	−0.4507	0.692
0.40	1.6821	0.3822	−0.0737	−1.0116	0.1722	1.5184	−0.1955	0.1099	−0.4734	0.695
0.45	1.6139	0.3822	−0.0861	−0.9939	0.1722	1.5184	−0.2011	0.1178	−0.4927	0.699
0.50	1.5288	0.3822	−0.0960	−0.9755	0.1722	1.5184	−0.2089	0.1142	−0.5035	0.699
0.60	1.3081	0.3822	−0.1133	−0.9407	0.1722	1.5184	−0.2212	0.1016	−0.5546	0.704
0.70	1.1383	0.3822	−0.1292	−0.9193	0.1722	1.5184	−0.1900	0.1036	−0.6037	0.710
0.80	1.0757	0.3822	−0.1442	−0.9167	0.1722	1.5184	−0.1865	0.1058	−0.6319	0.718
0.90	0.9935	0.3822	−0.1577	−0.9104	0.1722	1.5184	−0.1643	0.1165	−0.6577	0.723
1.00	0.8642	0.3822	−0.1687	−0.9001	0.1722	1.5184	−0.1505	0.1372	−0.6916	0.728
1.50	0.3150	0.3822	−0.2006	−0.8696	0.1722	1.5184	−0.0377	0.1572	−0.7582	0.738
2.00	−0.1760	0.3822	−0.2190	−0.8328	0.1722	1.5184	0.0780	0.1660	−0.7863	0.726
2.50	−0.4103	0.3822	−0.2319	−0.8415	0.1722	1.5184	0.0907	0.1648	−0.7939	0.709
3.00	−0.5019	0.3822	−0.2431	−0.8684	0.1722	1.5184	0.1195	0.1790	−0.7754	0.707
3.50	−0.7206	0.3822	−0.2479	−0.8689	0.1722	1.5184	0.1206	0.1629	−0.7673	0.708
4.00	−0.9383	0.3822	−0.2493	−0.8618	0.1722	1.5184	0.1267	0.1262	−0.7457	0.707
4.40	−1.0405	0.3822	−0.2559	−0.8472	0.1722	1.5184	0.1655	0.1486	−0.7042	0.717
5.00	−1.3694	0.3822	−0.2535	−0.8287	0.1722	1.5184	0.2208	0.1648	−0.6955	0.715

indicate the largest amplitude for intraslab events than interface ones when the magnitude and the hypocentral distance are the same. Since the GMPEs of Lin and Lee (2008) are among the only GMPEs from the regression of ground motion observations in Taiwan, they were applied to this study.

Seismic Hazards in Taiwan

The Hazard Maps

By considering all of the seismogenic sources, the corresponding parameters, and the GMPEs, a PSHA was applied for Taiwan. The spatial distributions of seismic hazards were evaluated in the form of a seismic hazard map. The seismic hazards for 10 % (475-year return period) and 2 % (2,475-year return

DOI 10.1007/978-3-642-36197-5_100-1

Table 8 The corresponding parameters and the standard deviations (σ_{lny}) of the GMPEs for the PGA and each response period for subduction events (Eq. 9) as proposed by Lin and Lee (2008)

Period	C1	C2	C3	C4	C5	C6	C7	σ_{lny}
PGA	−0.9000	1.0000	−1.9000	0.9918	0.5263	0.0040	0.3100	0.6277
0.010	−2.2000	1.0850	−1.7500	0.9918	0.5263	0.0040	0.3100	0.5800
0.020	−2.2900	1.0850	−1.7300	0.9918	0.5263	0.0040	0.3100	0.5730
0.030	−2.3400	1.0950	−1.7200	0.9918	0.5263	0.0040	0.3100	0.5774
0.040	−2.2150	1.0900	−1.7300	0.9918	0.5263	0.0040	0.3100	0.5808
0.050	−1.8950	1.0550	−1.7550	0.9918	0.5263	0.0040	0.3100	0.5937
0.060	−1.1100	1.0100	−1.8360	0.9918	0.5263	0.0040	0.3100	0.6123
0.090	−0.2100	0.9450	−1.8900	0.9918	0.5263	0.0040	0.3100	0.6481
0.100	−0.0500	0.9200	−1.8800	0.9918	0.5263	0.0040	0.3100	0.6535
0.120	0.0550	0.9350	−1.8950	0.9918	0.5263	0.0040	0.3100	0.6585
0.150	−0.0400	0.9550	−1.8800	0.9918	0.5263	0.0040	0.3100	0.6595
0.170	−0.3400	1.0200	−1.8850	0.9918	0.5263	0.0040	0.3100	0.6680
0.200	−0.8000	1.0450	−1.8200	0.9918	0.5263	0.0040	0.3100	0.6565
0.240	−1.5750	1.1200	−1.7550	0.9918	0.5263	0.0040	0.3100	0.6465
0.300	−3.0100	1.3150	−1.6950	0.9918	0.5263	0.0040	0.3100	0.6661
0.360	−3.6800	1.3800	−1.6600	0.9918	0.5263	0.0040	0.3100	0.6876
0.400	−4.2500	1.4150	−1.6000	0.9918	0.5263	0.0040	0.3100	0.7002
0.460	−4.7300	1.4300	−1.5450	0.9918	0.5263	0.0040	0.3100	0.7092
0.500	−5.2200	1.4550	−1.4900	0.9918	0.5263	0.0040	0.3100	0.7122
0.600	−5.7000	1.4700	−1.4450	0.9918	0.5263	0.0040	0.3100	0.7280
0.750	−6.4500	1.5000	−1.3800	0.9918	0.5263	0.0040	0.3100	0.7752
0.850	−7.2500	1.5650	−1.3250	0.9918	0.5263	0.0040	0.3100	0.7931
1.000	−8.1500	1.6050	−1.2350	0.9918	0.5263	0.0040	0.3100	0.8158
1.500	−10.3000	1.8000	−1.1650	0.9918	0.5263	0.0040	0.3100	0.8356
2.000	−11.6200	1.8600	−1.0700	0.9918	0.5263	0.0040	0.3100	0.8474
3.000	−12.6300	1.8900	−1.0600	0.9918	0.5263	0.0040	0.3100	0.8367
4.000	−13.4200	1.8700	−0.9900	0.9918	0.5263	0.0040	0.3100	0.7937
5.000	−13.7500	1.8350	−0.9750	0.9918	0.5263	0.0040	0.3100	0.7468

period) of the probability of exceedance for 50 years are presented (Fig. 9). The results suggest that seismic hazards in Taiwan are mainly contributed by active fault sources. The highest seismic hazard levels were determined from the Western Foothills to the Coastal Plain. A >1.0 *g* hazard for a 10 % probability of exceedance for 50 years was estimated near the Chiayi blind fault and the Tachienshan Fault (Fig. 9a). A high hazard was also evaluated along the eastern coastline and can be attributed to crustal active fault sources with short recurrence intervals along the Longitudinal Valley (Fault ID 26–33 in Table 3). In contrast, in northern Taiwan, a low hazard level was obtained. Although the Sanchiao Fault is located in this region, the recurrence intervals of the fault are rather long (in between 614 and 2,511 years).

The Hazard Curves

In order to represent the probability of annual exceedance as a function of ground motion level for different response periods, hazard curves are presented. The hazard curves were evaluated for the six municipalities, i.e., the Taipei, New Taipei, Taoyuan, Taichung, Tainan, and Kaohsiung Cities, respectively (Fig. 10). The hazard curves for PGA and the response period of 0.3 and 1.0 s are obtained. Since some active faults are close to the Tainan and Taichung Cities (Fig. 9), higher hazards were determined.

Encyclopedia of Earthquake Engineering
DOI 10.1007/978-3-642-36197-5_100-1

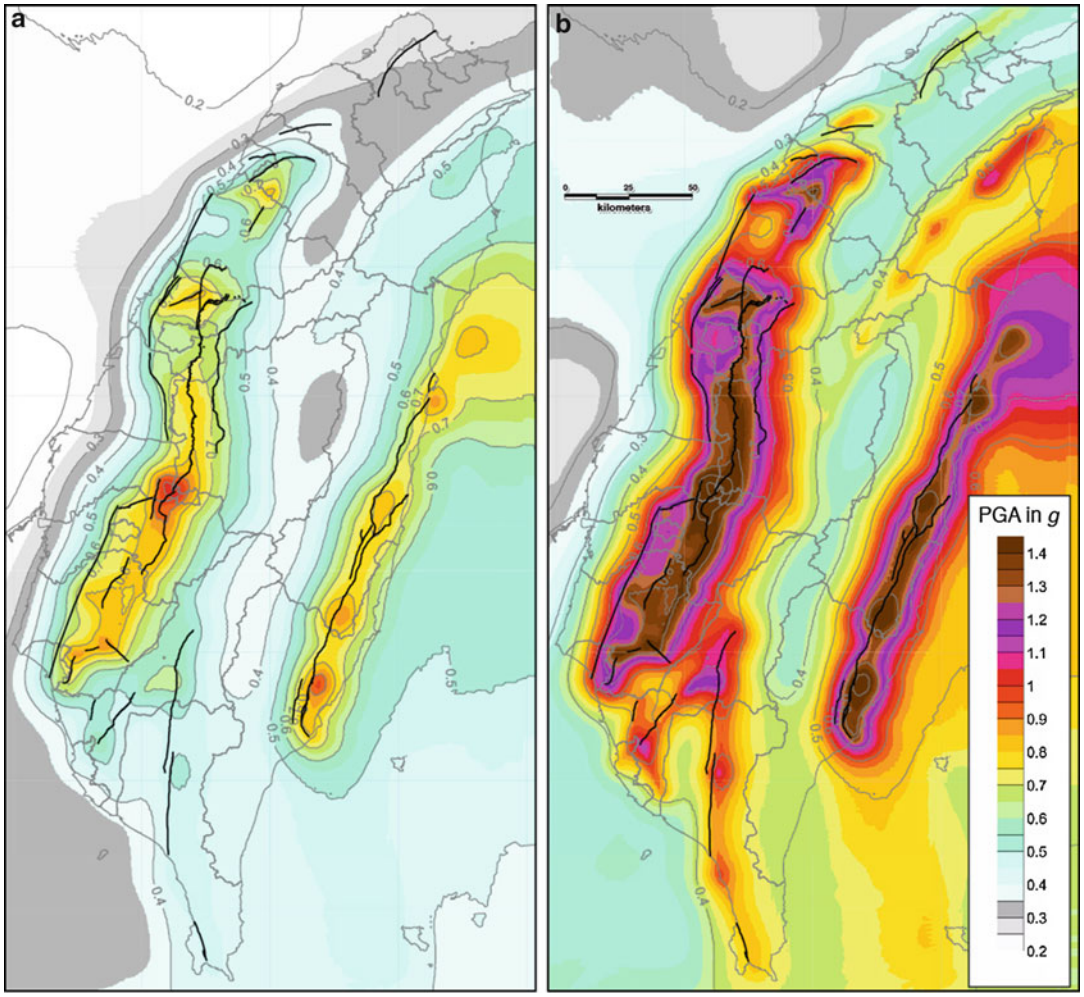

Fig. 9 The seismic hazard maps in (**a**) a 10 % (a 475-year return period) and (**b**) a 2 % (a 2,475-year return period) probability of exceedance for 50 years

By contrast, the hazards in the Taipei, New Taipei, Taoyuan, and Kaohsiung cities are relatively low because of they are further away from crustal active fault sources with short recurrence intervals.

Discussion and Conclusions

A Comparison to Other PSHA Results

Probabilistic seismic hazards imparted by different seismogenic sources for the Taiwan region were assessed. Higher hazards were determined along active faults in the Coastal Plain and the Longitudinal Valley. The pattern can be associated with the distribution of seismic activity in Taiwan. The pattern is similar to those obtained from previous studies (e.g., Cheng et al. 2007). In more detail, hazard peaks were evaluated near crustal active fault sources with short recurrence intervals. The results were similar to those obtained from other PSHA studies (e.g., Campbell et al. 2002; Cheng et al. 2007), which also considered the hazards imparted by active faults. The pattern can be attributed to the behaviors of GMPEs (Lin 2009), illustrating the significance of larger ground shakings surrounding regions close to earthquake epicenters or rupture faults. The attenuation behavior is similar to observations of the 1999 Chi-Chi, Taiwan,

DOI 10.1007/978-3-642-36197-5_100-1

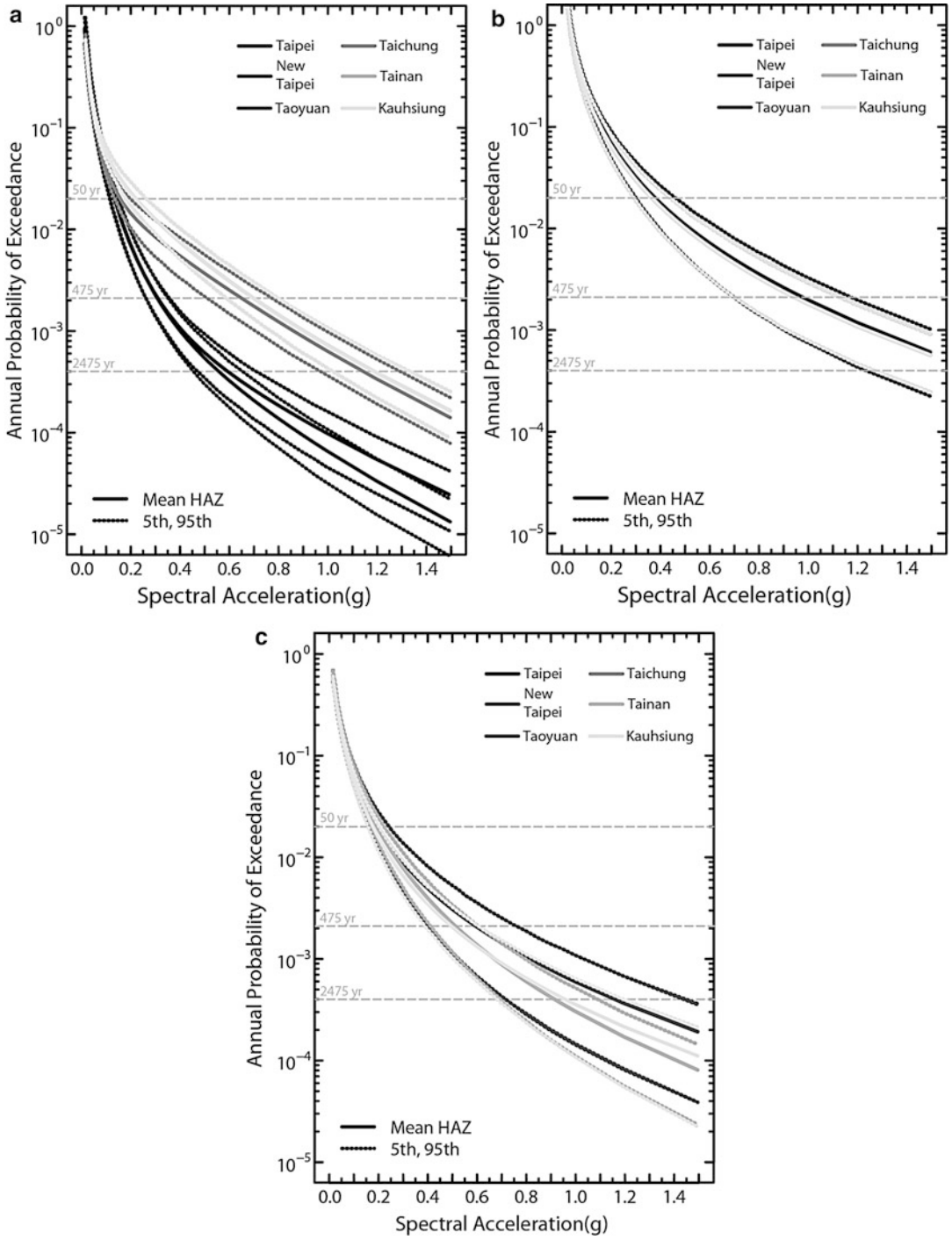

Fig. 10 The probability of annual exceedance as a function of hazard curves for PGA and the response period of 0.3 and 1.0 s for the six municipalities. The *solid* and *dashed lines* represent mean and two standard deviations of seismic hazards, respectively

earthquake. The shake map of this earthquake indicated significant high ground shakings in the form of PGA in the vicinity of the Chelungpu Fault, which ruptured during the coseismic period.

DOI 10.1007/978-3-642-36197-5_100-1

The Importance of the Short-Term Probabilistic Seismic Hazard Assessment

Recently, the concept of a traditional PSHA has been called into question. One of the standard procedures for traditional PSHAs is the construction of return periods for characteristic earthquakes that are independent of one another (see section "The Declustering Process" for details). Thus, an earthquake should be declustered prior to its incorporation for a PSHA. However, some recent cases have determined disadvantages for traditional PSHAs. For example, the M_w 6.3, 21 February 2011, Christchurch earthquake can be regarded as an aftershock of the M_w 7.1 Darfield earthquake that took place on 4 September 2010. The Christchurch earthquake caused severe damage in downtown Christchurch due to a closer epicentral distance. Additionally, not only can aftershocks lead to devastating seismic hazards, but the next earthquake could expand hazards. An earthquake with a M_w 7.4 took place off the Pacific coast of Tohoku, Japan, on 9 March 2011. Due to its distance from urban regions, the resulting damage from this earthquake was negligible. Fifty-one hours after the earthquake (on March 11), a M_w 9.1 earthquake took place in the vicinity and resulted in disasters in Japan. Seismic hazards may also result from several events within an earthquake sequence. Based on spatial and temporal relationships, the 1904 Touliu and the 1906 Yanshuigang earthquakes can be regarded as a foreshock and an aftershock of the 1906 Meishan earthquake (Fig. 2), respectively. However, all three earthquakes caused severe disasters. The case indicates the importance of the seismic hazards imparted by each event in an earthquake sequence and raises the unsuitability of traditional PSHAs (Chan et al. 2013b). Such instances indicate the importance of an earthquake sequence in respect to seismic hazard evaluations and suggest the reevaluation of seismic hazards immediately following large earthquakes.

Several studies have recognized disadvantages in traditional PSHAs and have considered a time dependency for PSHAs. For example, Chan and Wu (2012) and references therein estimated the temporal evolution of the seismicity rate and assessed seismicity hazards as a function of time. The feasibility of this approach has been tested using applications to several cases in Taiwan (e.g., Chan et al. 2013a, b).

The Applicability of PSHA Results and Seismogenic Parameters

An assessment of seismic hazards had been widely applied for each administrative region in Taiwan. In addition, hazard curves for the six municipalities were evaluated. According to the results, the probability of annual exceedance as a function of ground motion level for different response periods was presented. They would be valuable to lawmakers for determining building codes and to decision-makers for the site selection of public structures.

In addition, based on the PSHA results, further applications in respect to seismic hazard mitigation can be assessed (e.g., probabilistic seismic risk assessment). A risk assessment is presented as the probability that a given loss of property and human life exceeds a specific value during a time period. For its application, seismic hazards, exposure (distribution of population or construction), and a corresponding vulnerability are incorporated. The result could be of benefit to decision-makers for territorial planning.

The parameters implemented for the PSHA were acquired through the integration of state-of-the-art information regarding the tectonic setting, geology, geomorphology, earthquake catalog, geophysics, and the ground motion attenuation. The information could be used as a reference for an additional PSHA. For example, these parameters will be regarded as a branch in the logic tree approach for the Committee of Taiwan Earthquake Model (TEM, http://tec.earth.sinica.edu.tw/TEM). TEM is working on a seismic hazard map for the entire region of Taiwan. In the meantime, the work can also be incorporated within the Global Earthquake Model (see entry "The Global Earthquake Model (GEM)"), integrated by several research institutes, insurance, and reinsurance enterprises in order to evaluate seismic hazards around the world. Through collaboration with organizations on different scales and with different individuals, the GEM is expected to establish uniform and open standards for calculating and communicating earthquake hazards and risks worldwide.

DOI 10.1007/978-3-642-36197-5_100-1

Summary

A probabilistic seismic hazard assessment is implemented to the region of Taiwan. Seismogenic sources, which may result in seismic hazards, were divided into the following categories: shallow-crust regional sources, deep-crust regional sources, crustal active fault sources, subduction intraslab sources, and subduction interface sources. By further considering ground motion prediction equations for different types of sources and site conditions, hazard maps in Taiwan and hazard curves in the six municipalities were assessed.

Cross-References

► Earthquakes and Tectonics: An Observation from Taiwan
► Probabilistic Seismic Hazard Assessment: An Overview

References

Arabasz WJ, Robinson R (1976) Microseismicity and geologic structure in the northern south island, New Zealand. J Geol Geophys 19:569–601

Campbell KW, Thenhaus PC, Barnard TP, Hampson DB (2002) Seismic hazard model for loss estimation and risk management in Taiwan. Soil Dyn Earthq Eng 22:743–754. doi:10.1016/S0267-7261(02)00095-7

Chan CH, Wu YM (2012) The burst of seismicity after the 2010 M6.4 Jiashian earthquake and its implication of short-term seismic hazard in southern Taiwan. J Asian Earth Sci 51:231–239. doi:10.1016/j.jseaes.2012.08.011

Chan CH, Wu YM, Cheng CT, Lin PS, Wu YC (2013a) Time-dependent probabilistic seismic hazard assessment and its application to Hualien City, Taiwan. Nat Hazards Earth Syst Sci 13:1–16. doi:10.5194/nhess-13-1-2013

Chan CH, Wu YM, Cheng CT, Lin PS, Wu YC (2013b) Scenario for a short-term probabilistic seismic hazards assessment (PSHA) in Chiayi, Taiwan. Terr Atmos Ocean Sci 24(4, Part II):671–683. doi:10.3319/TAO.2013.01.22.01(T)

Chen C-H, Wang J-P, Yih-Min W, Chan C-H, Chang C-H (2012) A study of earthquake inter-occurrence times distribution models in Taiwan. Nat Hazards. doi:10.1007/s11069-012-0496-7

Cheng CT, Chiou SJ, Lee CT, Tsai YB (2007) Study on probabilistic seismic hazard maps of Taiwan after Chi-Chi earthquake. J Geo Eng 2:19–28

Cornell CA (1968) Engineering seismic risk analysis. Bull Seismol Soc Am 58(5):1583–1606

Gardner JK, Knopoff L (1974) Is the sequence of earthquakes in southern California, with aftershocks removed, poissonian? Bull Seismol Soc Am 64:1363–1367

Gutenberg B, Richter C (1954) Seismicity of the earth and associated phenomena, 2nd edn. Princeton University Press, Princeton, 310

Hanks TC, Kanamori H (1979) A moment magnitude scale. J Geophys Res 84:2348–2350

Hsu Y-J, Yu S-B, Simons M, Kuo L-C, Chen H-Y (2009) Interseismic crustal deformation in the Taiwan plate boundary zone revealed by GPS observations, seismicity, and earthquake focal mechanisms. Tectonophysics 479:4–18

Kiureghian AD, Ang AH-S (1977) A fault- rupture model for seismic risk analysis. Bull Seismol Soc Am 67:1173–1194

DOI 10.1007/978-3-642-36197-5_100-1

Kramer SL (1996) Geotechnical earthquake engineering. Prentice Hall, Upper Saddle River, 653 pp

Lin PS (2009) Ground-motion attenuation relationship and path-effect study using Taiwan Data set. PhD dissertation, Institute of Geophysics, National Central University, Chung-Li, Taiwan (in Chinese)

Lin PS, Lee CT (2008) Ground-motion attenuation relationships for subduction-zone earthquakes in northeastern Taiwan. Bull Seismol Soc Am 98(1):220–240. doi:10.1785/0120060002

Tsai YB, Wen KL, Chen KB, Kuo JY (2000) Summary of development of the Taiwan earthquake catalog and strong ground motion attenuation equations. Report for the National Project on the Disaster Prevention, 79 pp (in Chinese)

Uhrhammer RA (1986) Characteristic of northern and central California seismicity. Earthquake Notes 57(1):21 (Abstract)

Wesnousky SG (1994) The Gutenberg-Richter or characteristic earthquake distribution, which is it? Bull Seismol Soc Am 84:1940–1959

Wu YM, Hsu YJ, Chang CH, Teng LS, Nakamura M (2010) Temporal and spatial variation of stress field in Taiwan from 1991 to 2007: insights from comprehensive first motion focal mechanism catalog. Earth Planet Sci Lett 298:306–316. doi:10.1016/j.epsl.2010.07.047

Wyss M (1979) Estimating maximum expectable magnitude of earthquakes from fault dimensions. Geology 7:336–340

Youngs RR, Coppersmith KJ (1985) Implications of fault slip rates and earthquake recurrence models to probabilistic seismic hazard estimates. Bull Seismol Soc Am 75:939–964